A Cancer Diagnostics Biosensor System Based on Micro- and Nano-technologies

Pedro Ortiz[1], Neil Keegan[1], Julia Spoors[1], John Hedley[1], Alun Harris[1], Jim Burdess[1], Richie Burnett[1], Margit Biehl[2], Werner Haberer[2], Thomas Velten[2], Matthew Solomon[3], Andrew Campitelli[3], and Calum McNeil[1]

[1] Newcastle University, Newcastle upon Tyne, UK
[2] Fraunhofer Institute for Biomedical Engineering (IBMT), Sankt Ingbert, Germany
[3] MiniFAB Pty Ltd., Victoria, Australia
p.m.ortiz@ncl.ac.uk, neil.keegan@ncl.ac.uk

Abstract. A biosensor system for medical diagnostics based around resonant MEMS sensor technology is presented in this paper. The working principle of the bioMEMS device is introduced and the functionalisation strategies for cancer marker recognition are described. In addition, the successful packaging and integration of functional MEMS biosensor devices are reported herein. This ongoing work represents one of the first hybrid assemblies to integrate a PCB packaged silicon MEMS device into a disposable microfluidic device.

Keywords: Lab-on-a-Chip, microfluidics, bioMEMS, biosensors, clinical diagnostics, packaging.

1 Introduction

A silicon MEMS biosensor which is integrated into a polymer-based microfluidic system will be presented. This hybrid module uses Micro- and Nano-technologies to integrate a functional bioMEMS device with state-of-the-art printed circuit board (PCB) packaging and microfluidics. This microfluidic cartridge is part of a point-of-care instrument for cancer diagnostics and monitoring being developed within the European Commission funded project, SmartHEALTH [1].

1.1 CDR Working Principle

The MEMS device presented is a Circular Diaphragm Resonator (CDR) [2-4] which is enabled for biomolecule immobilisation using standard gold-thiol surface chemistry or a novel 3-dimensional, bio-active polymer matrix [5]. The CDR device takes advantage of the degenerate mode resonant mass sensor principle [3]. In short, this principle, illustrated in Figure 1, consists of a vibrating circular diaphragm which supports a pair of spatially independent modes of vibration that share a common natural frequency. When the area corresponding to one of these modes is functionalised with a biological capture species e.g. an antibody, while the rest of the surface remains inert,

A. Schmid et al. (Eds.): Nano-Net 2009, LNICST 20, pp. 169–177, 2009.

a change in mass as a result of target biomolecule binding on the functionalised area results in a split in the resonant frequency of the two modes. The resulting frequency split is proportional to the mass added specifically to the functionalised area. This type of structure presents the intrinsic advantage of having a reference frequency, to compensate for non-specific effects, within the same structure of the functional device thus improving the sensitivity of detection.

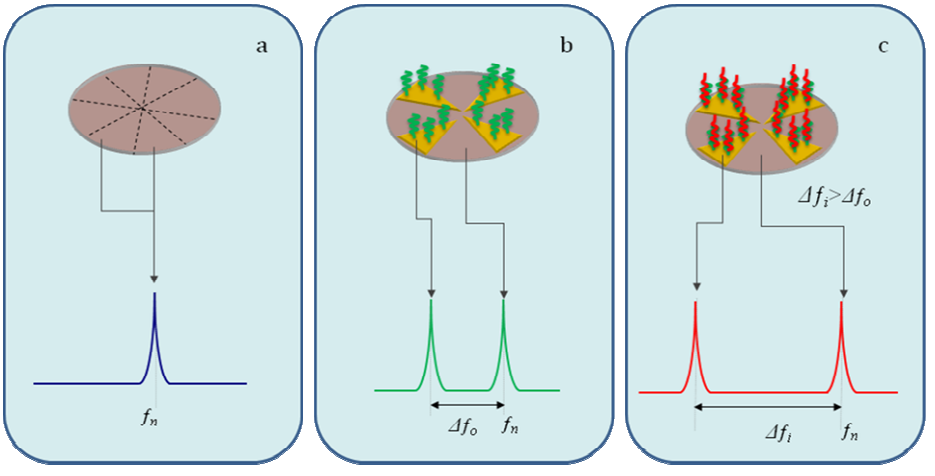

Fig. 1. Schematic representation of the CDR sensor concept: a) A homogeneous diaphragm clamped at the edges presents two spatially independent modes of vibration which share a common natural frequency. b) A frequency split is created between the two modes by the site specific mass added during functionalisation. c) Supplementary addition of mass when the target analyte is captured further increases the frequency split.

2 BioMEMS Device Fabrication and Cartridge Assembly

A new fabrication process for the CDR device was developed in conjunction with Tronics Microsystems (France). The MEMS devices consist of two bonded silicon on insulator (SOI) substrates: A base SOI wafer with a highly doped device layer which is patterned and etched to the buried oxide (BOX) to form the actuation/sense electrodes, and a top SOI substrate oxidised, patterned, etched and then bonded to the base substrate. The handle wafer and the BOX of the top SOI substrate are then etched to form the 4 µm thick, <111> silicon diaphragm as shown in Figure 2.

This newly developed fabrication process differs from what has been previously reported [6], as the glass base substrate is replaced by the base SOI substrate. The new design means that metal electrodes are replaced by highly doped silicon ones on the device layer of the base SOI wafer. This feature has allowed the production of sealed dies thanks to the inclusion of a bonding perimeter in the new device's layout. This is translated into devices with low internal pressures (~6×10^{-4} mbar which is the wafer bonding chamber pressure); in contrast to glass base wafer devices. The new chips are

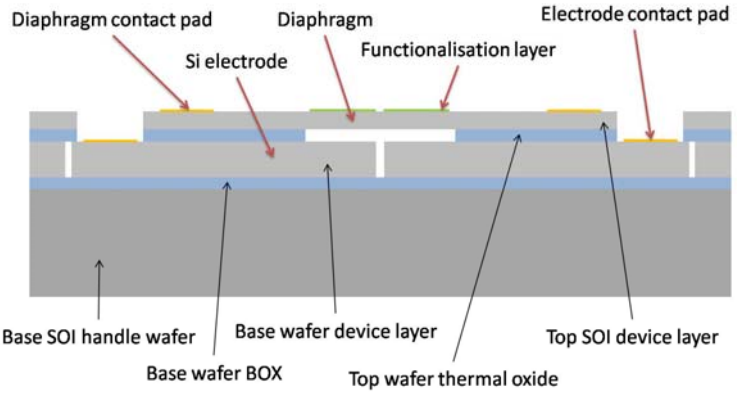

Fig. 2. Schematic cross-section of the MEMS devices fabricated by Tronics Microsystems. Theses devices have a 4 µm thick diaphragm with a diameter of 240 µm and the overall die size is 2.2 mm × 2.2 mm.

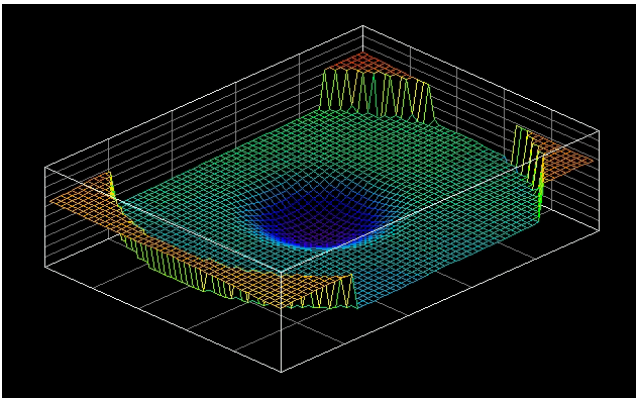

Fig. 3. Surface profile of a bare CDR device. In this image it can be appreciated that the diaphragm presents a concave surface. This deflection of the diaphragm is caused by a pressure difference between the CDR cavity and the external atmospheric pressure.

slightly larger than previously integrated ones (2.2 mm × 2.2 mm, compared to 2 mm × 2 mm [6]) to increase the bonding area of the sealing perimeter of the die. Figure 3 shows the surface profile of a bare CDR device (obtained using a Zygo, NewView 7000 surface profiler), from this image it can be clearly appreciated that the diaphragm presents a concave surface. This appearance is the product of diaphragm deflection caused by a pressure difference between the inside of the CDR cavity and the external atmospheric pressure, thus indicating that the die is indeed sealed at low internal pressure.

A further advantage of the new fabrication process is that an additional lithography step and chromium/gold patterning have been included. This allows, in a single wafer, a portion of the devices (1/3) to be enabled for biological functionalised through well

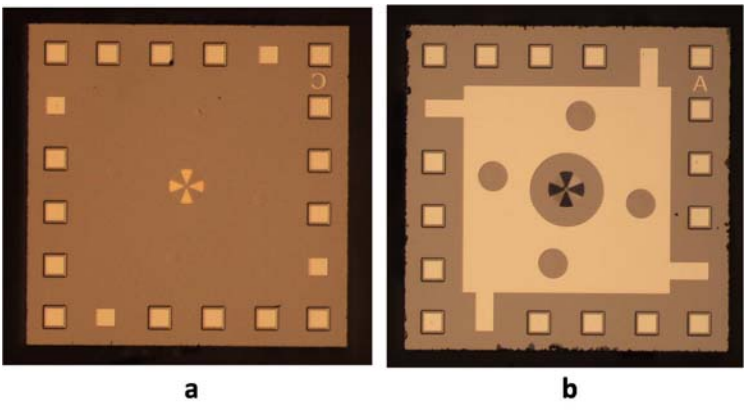

Fig. 4. CDR devices showing realised functionalisation patterns in the centre of the die, a) a CDR with chromium/gold functionalisation pattern and b) a CDR with an APTES polymer pattern for subsequent bio-activation. The CDR die on the right also has a diaphragm metal layer covering a large portion of the surface for better electrical shielding.

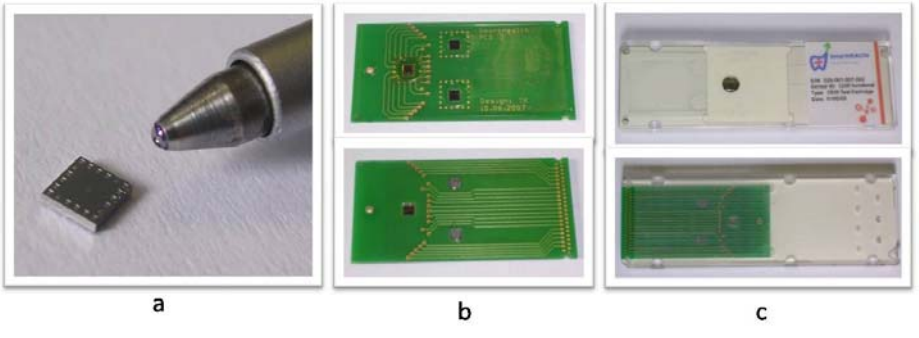

Fig. 5. a) A CDR chip. b) Front (top) and back (bottom) of a CDR-loaded PCB. For development purposes only one device is wired at this stage. c) Microfluidic cartridge containing the CDR-loaded PCB.

established gold-thiol immobilisation chemistry [8], while the remaining devices are patterned with APTES polymer using a lift-off process [5]. Figure 4 shows dies with the two types of functionalisation layer.

The CDR sensor die (Figure 5, a) has been successfully packaged into a custom PCB shown in Figure 5, b. This represents a considerable milestone since the functionalised diaphragm is a very delicate structure and must remain clear and untouched at all times during the packaging process. In the near future the PCB will house the necessary electronic components to drive the diaphragm and to detect the output signal; this system is currently being developed at Newcastle University. This PCB packaging concept has been developed by the Fraunhofer IBMT [7]. Devices produced using the previous fabrication process (glass base substrate) required that during integration, the bond pads remained uncovered by encapsulating epoxy as any

air trapped in the cavity resulted in diaphragm vibration damping; this is not the case with the new fabrication process which are sealed with low internal pressure. Finally, the CDR-loaded PCB is incorporated into a microfluidic cartridge (Figure 5, c), developed by MiniFAB, which is compatible with the design constraints of the overall SmartHEALTH instrument.

3 Device Functionalisation: Surface Chemistry and Biopatterning

A hydrophilic polymer was developed as an alternative to the widely used thiol-gold surface chemistry for biological functionalisation. Using novel conditions for deposition, APTES was shown to form a porous polymeric capture network covalently linked to silicon surfaces. The porous layer can be deposited with a controlled thickness between 100 nm and 5 µm, far exceeding the monolayer surface chemistry previously reported in the literature [9]. Firstly, the hydrophilic nature of the polymer helps to maintain the 3-D structure of biomolecules and therefore improves functionality at the sensor interface. Secondly, and most importantly, the polymer has demonstrated the ability to absorb biomolecules throughout its porous structure, which should increase the dynamic range of the sensor. Finally, the optimised chemistry on CDR patterns has demonstrated that the immobilisation strategy produces highly site-specific and reproducible surfaces for both CEA antigen / HPV DNA target recognition. Both species are important markers for cancer diagnostics and will be used in conjunction with the polymer and test cartridge in the analytical assessment of the BioMEMS clinical diagnostic system. In addition, it has been demonstrated that the polymer has wide applicability to bio-molecule capture, signposting a new platform technology for generic immobilisation. Figure 6 shows a step-by-step development guide to the surface chemistry and its capture capabilities as follows: A.) A photolithographic mask was manufactured. B.) The mask acts as a stencil to divide the CDR diaphragm into four sections of exposed silicon in photoresist background. C/D.) After photoresist removal, SEM images demonstrate the successful deposition of polymer within the defined CDR pattern. The depth of polymer deposition was controllable using different incubation times. E.) A characteristically well defined polymer pattern visualised by autofluorescence at ~ 520 nm. F.) The tagged probe molecule AntiCEA-Alexa647 fluoresces at 650 nm and shows an identical defined pattern to the underlying polymer layer after a short incubation. The four non-recruiting sections can be either left bare or filled with a blocking molecule. G/H.) The two confocal microscopy images of a slice taken across a polymer arm indicate that the probe molecule was absorbed throughout the porous polymer structure as well as adsorbed at the surface. The autofluorescence of the polymer layer indicated a 4µm z-axis height and the AntiCEA-Alexa647 absorbed fluorophore indicated a virtually identical height I.) The top polymer pattern was activated with native AntiCEA/ blocking solution and used to successfully bind CEA tagged with Alexa647. The bottom polymer pattern was only backfilled with blocking solution and resulted in no CEA recognition. It is noteworthy that preliminary stability studies have indicated that the polymer is stable over a 50 day period and the probe antibody remains stable within the polymer matrix for over 50 days at room temperature.

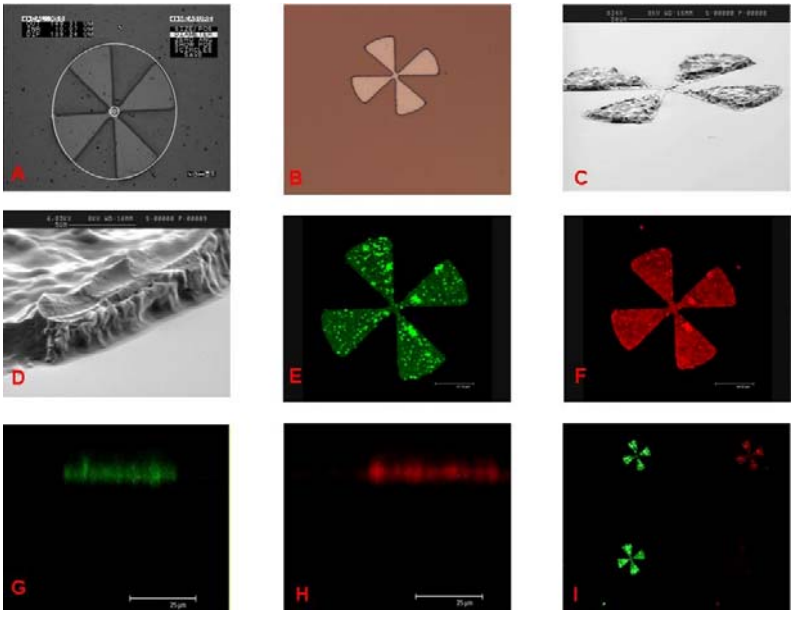

Fig. 6. Overview of CDR surface chemistry and biopatterning development, from photolithography mask (A) to resist patterning (B) selective deposition of APTES by polymer lift-off (C, D and E), successful absorption of Alexa647 tagged AntiCEA on the 3-D structure (F, G and H) and finally successful recognition of CEA antibody and control (I)

The CDR patterned with gold will undergo a conventional immobilisation protocol using a mixed monolayer of thiols. This provides an alternative route to analytical data should the novel polymer system prove to be inappropriate. The initial thiol system will rely on a 90:10 mix of protein resistant thiol spacer ($HS\text{-}(CH_2)_{11}\text{-}EG_3OH$) and thiol linker ($HS\text{-}(CH_2)_{11}\text{-}EG_6\text{-}NH_2$), but the concentration of linker may be increased after empirical work. Polyethylene glycol molecules are well reported in the literature as protein resistant and are used here to reduce non-specific background in our sensor systems. The thiol linker molecule will be used to bind biomolecules of interest using the specific reactive groups presented from the monolayer. An NH_2 terminal group is intended to bind molecules that have been activated with a NHS ester, however, the linker could be changed to a carboxy or hydrazide group and molecules containing amines or carbohydrates bound to the surface. Another possibility is to present biotin as the reactive surface species and build up the surface using streptavidin and molecules of interest tagged with biotin. Figure 7 shows a schematic of the alternative thiol chemistries that will be employed on gold patterned CDR. The base layer chemistry used to bind specific recognition molecules will be assessed on a case by case basis and the linker molecules used in a reaction scheme that spawns oriented bio-molecule immobilisation.

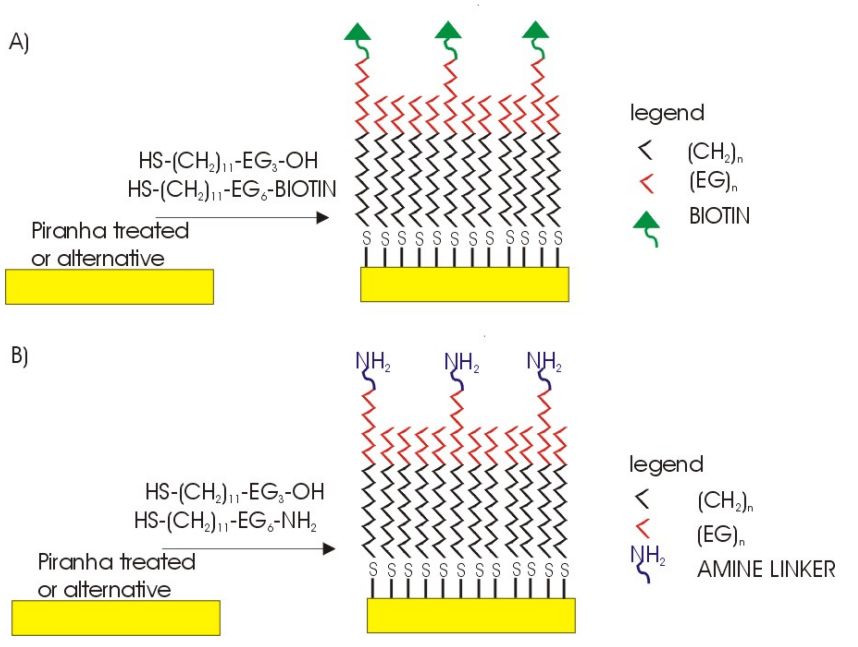

Fig. 7. Schematic representations of base layer chemistries on gold surfaces. Scheme A) binds subsequent layers through biotin interactions. Scheme B) is intended to bind molecules that have been activated with a NHS ester. However, the linker could be changed to a carboxy or hydrazide group and molecules containing amines or carbohydrates bound to the surface. In both schemes the EG regions are intended to limit non-specific background.

4 Preliminary CDR Performance Assessment

Initial testing of non-functionalised CDR devices (i.e. devices with a completely bare diaphragm as depicted on Figure 1, a) was carried out with a laser Doppler vibrometry station, an actuation voltage of 10 V_{pp} (DC offset of 5 V) and at 0.1 mbar. The results obtained revealed an intrinsic split in the natural frequencies of the sense and reference modes. This intrinsic split can be observed in Figure 8, which shows a typical CDR response. This phenomenon is attributed to SOI wafer and device manufacturing imperfections which induce small diaphragm thickness variations. A sample of eight devices was evaluated and an average of 3.56 MHz and 3.57 MHz were obtained for the sense and reference modes respectively. The standard deviation was 0.101 MHz for both modes. The average Δf_0 was 14.25 kHz, which if compared to the 154 kHz Δf_0 obtained with the glass base substrate CDR reveals that the new devices are closer to degeneracy (which is only attained in the ideal case)[3].

The mass added by the by the chromium/gold (50 Å chromium, 500 Å gold) functionalisation pattern was used for a preliminary assessment of CDR performance. An average Δf_0 of 96.15 kHz was measured on a sample of ten CDR devices (under that same test conditions mentioned above) with chromium/gold functionalisation pattern (before biomolecule immobilisation), with a standard deviation of 5.09 kHz. A typical sensor response is shown in Figure 9. This represents a change in Δf of 81.9 kHz with

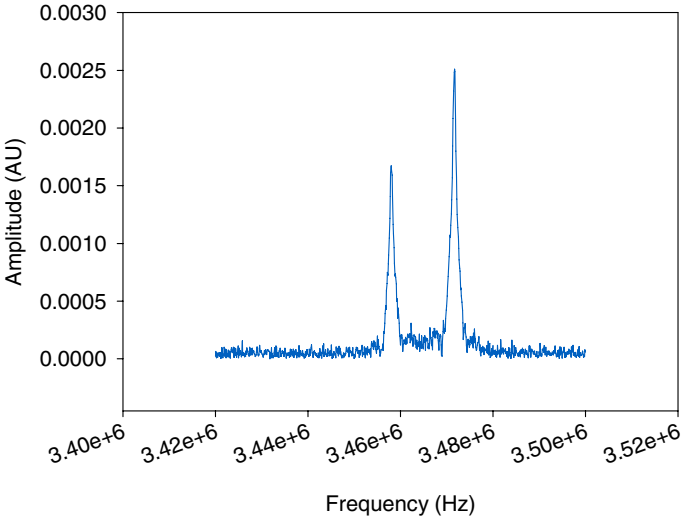

Fig. 8. Typical bare CDR response. The figure shows an intrinsic natural frequency split of 13.9 kHz between the two spatially independent modes of vibration which serve as sense and reference.

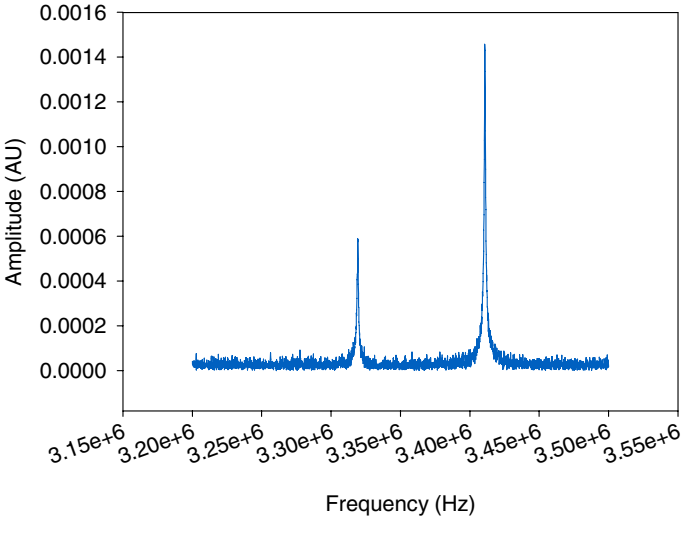

Fig. 9. Typical response of a CDR with gold chromium/gold functionalisation pattern. It this case the sense mode resonant peak is found at 3.32 MHz and the reference mode is found at 3.41 MHz.

respect to the results obtained on bare CDR devices. The mass added to the surface of the diaphragm by the functionalisation pattern, covering 50 % of the diaphragm area (as can be seen in Figure 4, a) was calculated to be 22.64 ng. This means that the new CDR sensor response is 3.61 kHz for each nanogram of added metal. The base line

signal achieved with the new devices leaves us in a strong position to gain analytical data within fully packaged solutions in the near future.

5 Conclusions

The successful fabrication of a new generation of MEMS mass sensor devices based on the CDR principle has been presented. The new fabrication process implemented by Tronics Microsystems has successfully produced CDR devices with sealed diaphragm cavities at low internal pressure. Preliminary results obtained using the gold functionalisation pattern as added mass indicate that the CDR's response is of 3.61 kHz/ng. The ability to detect frequency shifts smaller than the above figure will ultimately dictate the sensitivity of the sensor, but this constitutes an encouraging stating point to achieve a sub-nanogram limit of detection.

The packaging and integration of the sensor chip onto a disposable microfluidic cartridge has also been presented. This hybrid assemblage of PCB packaged silicon MEMS and polymer microfluidics represents one of the first of its kind. The successful deposition of a bio-functionalizing polymer has also been achieved on the MEMS device thus converting it to a biosensor, which will be capable of detecting cancer markers at low levels. This will allow the SmartHEALTH project to proceed to proof of concept assays in the coming months.

Acknowledgments

The authors would like to thank the European Commission for providing the funds for the present work within the SmartHEALTH Integrated Project (FP6-2004-IST-NMP-2-016817).

References

1. http://www.smarthealthip.com
2. Burdess, J.S., McNeil, C.J.: 'Resonant Sensor' PCT Application PCT/GB2002/000237
3. Ismail, A.K., et al.: The principle of a MEMS circular diaphragm mass sensor. J. Micromech. Microeng. 16, 1487–1493 (2006)
4. Ismail, A.K., et al.: The fabrication, characterization and testing of a MEMS circular diaphragm mass sensor. J. Micromech. Microeng. 18(2), 1–10 (2008)
5. Suarez, G.: 'Immobilization of Biological Molecules' UK Patent Application 0513910.0
6. Ortiz, P., Keegan, N., Spoors, J., Hedley, J., Harris, J., Burdess, J., Burnett, R., Velten, T., Biehl, M., Knoll, T., Haberer, W., Solomon, M., Campitelli, A., McNeil, C.: Integration of a bioMEMS device into a disposable microfluidic cartridge for medical diagnostics. In: Proceedings of SPIE, Microfluidics, BioMEMS, and Medical Microsystems VII Conference, San Jose, CA, USA, January 24-29, vol. 7207 (2009)
7. Biehl, M., Haberer, W., Ortiz, P., Keegan, N., Spoors, J., Hedley, J., McNeil, C., Velten, T.: Packaging and integration of a micro-electro-mechanical silicon biochip. In: Proceedings of SPIE, Reliability, Packaging,Testing and Characterization of MEMS/MOEMS and Nanodevices VIII, San Jose, CA, USA, January 28-29, vol. 7206 (2009)
8. Bain, C.D., Whitesides, G.M.: Formation of monolayers by the coadsorption of thiols on gold: variation in the length of the alkyl chain. J. Am. Chem. Soc. 111(18), 7164–7175 (1989)
9. Ulman, A.: Formation and structure of self-assembled monolayers. Chem. Rev. 96, 1533–1554 (1996)